Triboelectric sensor as self-powered signal reader for scanning probe surface topography imaging

2015 Nanotechnology 26 165501

(http://iopscience.iop.org/0957-4484/26/16/165501)

IOP Publishing Nanotechnology
Nanotechnology 26 (2015) 165501 (8pp) doi:10.1088/0957-4484/26/16/165501

Triboelectric sensor as self-powered signal reader for scanning probe surface topography imaging

Aifang Yu[1,3], Libo Chen[1,3], Xiangyu Chen[1], Aihua Zhang[1], Fengru Fan[1], Yan Zhan[1] and Zhong Lin Wang[1,2]

[1] Beijing Institute of Nanoenergy and Nanosystems, Chinese Academy of Sciences, People's Republic of China
[2] School of Materials Science and Engineering, Georgia Institute of Technology, Atlanta, Georgia 30332-0245, USA

E-mail: zlwang@gatech.edu

Received 13 December 2014, revised 5 February 2015
Accepted for publication 5 March 2015
Published 31 March 2015

Abstract

We report a self-powered signal reading mechanism for imaging surface topography using a triboelectric sensor (TES) without supplying an external power or light source. A membrane-structured triboelectric nanogenerator (TENG) is designed at the root of a whisker (probe); the deflection of the whisker causes the two contacting surfaces of the TENG to give an electric output current/voltage that responds to the bending degree of the whisker when it scans over a rough surface. A series of studies were carried out to characterize the performance of the TES, such as high sensitivity of 0.45 V mm^{-1}, favorable repeating of standard deviation 8 mV, high Z-direction resolution of 18 μm, as well as lateral resolution of 250 μm by using a probe of size 11 mm in the length and 120 μm in radius. It not only can recognize the surface feature and size but also can perform a surface topography imaging in scanning mode. This work shows the potential of a TES as a self-powered tactile sensor for applications at relatively low spatial resolution.

Keywords: triboelectric nanogenerator, self-powered sensor, tactile sensor

(Some figures may appear in colour only in the online journal)

Introduction

Tactile sensing/imaging has vast applications in automatic control, remote operation, security systems, medical procedures, and advancing robotics [1–6]. The unique sensing functionalities of mammals and insects are tremendous attractive and have been aggressively emulated by smart electrical devices [7–11]. Mammalian whiskers present another important class of biosensors that can mediate tactile sensing for spatial mapping of nearby objects, monitor the airflow, and even enable balance during motion for advanced robotics with capabilities resembling those found in certain insects and mammals [12–14]. Various electronic whiskers based on different transduction methods, including piezoresistivity, optics, piezoelectricity, or capacitance, have been developed for various applications [11, 15–17]. All of these mechanisms rely on deformation of the sensing unit in response to the interaction of the whisker with a detected object. Compared to other sensors, electronic whiskers have high sensitivity and can be employed in hushed circumstances (dust, smoke, darkness), where the efficacy of other types of proximal sensing could be seriously compromised or limited/restricted. Nevertheless, a common limitation is that most of these sensors require an external power source or light source, which poses challenges to longevity and universality of this kind of sensor. New approaches are therefore necessary to overcome this limitation. Recently, a class of novelty self-powered sensors based on triboelectric nanogenerators

[3] Equal contribution to this work.

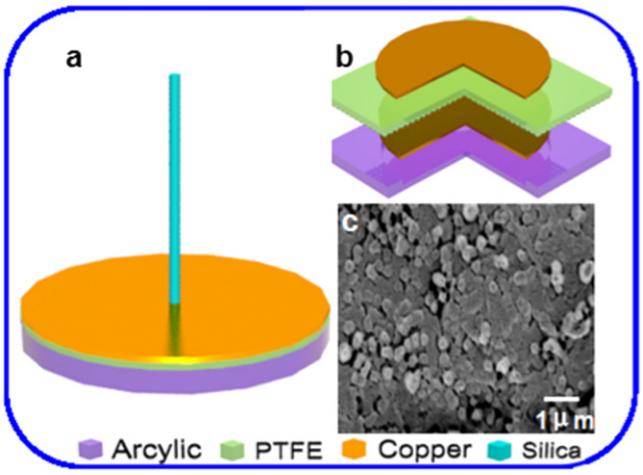

Figure 1. Structural design of the TES. (a) Schematic diagram of the sensor and (b) its cross-sectional view. (c) SEM image of PTFE nanoparticles structure fabricated on the film surface by ion plasma etching.

(TENGs) was invented [18]. By converting the mechanical stimulation from its working environment into a self-generated electric signal (current/voltage), the TENG-based sensors are able to work independently without an external power source. On the basis of a coupling of the universally known contact-electrification effect and electrostatic induction, TENGs have been extensively utilized to successfully build up cost effective and robust self-powered sensing systems with superior performance due to the excellent high output, such as velocity sensor [19], chemical sensor [20], pressure sensor [21], spatial displacement [22], acoustic sensor [23], etc [24].

In this paper, we present a novelty triboelectric sensor (TES) that consists of a whisker (probe) standing on the surface of a TENG in contact-separation mode. By scanning the whisker over a detected object, the distance between the two contact faces in the TENG will be modulated. A change in the gap distance results in an output electric signal because of the change in capacitance formed by the two surfaces that are electrostatically charged as a result of contact electrification. The magnitude reflects the degree at which the whisker was bent by the surface topography, and thus can be used to directly image the surface. This sensing unit is self-powered and doesn't rely on an external power supply, which will largely expand its application field.

Experimental section

The structure of the TES consists of two major parts: an artificial whisker (silica) and a TENG. The artificial whisker mounted at the center of the TENG sensing base has direct interaction with the detected object. A schematic of the sensor structure is illustrated in figure 1(a). Once an object contacts the whisker, transversally the whisker will be deflected or bent in response, which in turn causes the upper membrane of the TENG to be tilted or buckled. Based on a coupling of the contact-electrification effect and electrostatic induction, a buckling in the upper membrane will generate an electrical output due to the change of capacitance. For a better illustration, a cross-sectional view of the core is shown in figure 1(b), with a multilayered structure. A piece of acrylic sheet with a thickness of 3 mm was prepared by laser cutting as a substrate. At its center, a circular hole with depth of about 0.5 mm and diameter of 3.0 cm was fabricated by laser engraving. One layer of copper (Cu) with a thickness of 100 nm was deposited on the substrate as one contact face and electrode. The other contact face is a PTFE membrane with a deposited Cu thin film as the back electrode, which is adhered onto the acrylic substrate. The surface of PTFE was modified to create nanoparticle structure to further increase the surface roughness and the effective surface area of the TENG for effective triboelectrification by the inductively coupled plasma (ICP) reactive ion etching, as shown in figure 1(c). In the voltage measurement process, the TENG was connected with a Keithley 6514 system electrometer. In order to simplify the measurement process, the TES is at a standstill and the moving velocity of detected object was set at 1 mm s^{-1} in all measurements. The output current signals of the TENGs were measured by a low-noise current preamplifier (Stanford Research SR570). A KLA-Tencor D-100 surface profiler was used as a referred sensor.

Results and discussion

Figure 2 sketches the electricity generation mechanism of the TES. It can be explained by the coupling between the triboelectric effect and electrostatic induction. Because the PTFE membrane has a much more triboelectric negative polarity than that of the Cu contact face, electrons are injected from the Cu contact face into PTFE due to the contact-electrification from the previous cycles, generating positive triboelectric charges on the Cu contact face side and negative charges on the PTFE side. The negative and positive triboelectric charges are not annihilated, but remain on the surface of the PTFE membrane and Cu electrode for an extended period of time [25]. In order to better understanding the working mechanism of the sensor, the equivalent circuit of the sensor is also given. The TENG could be considered as two capacitors connected in parallel. Here, C_1 and C_2 represent the capacitance value of the left-hand and right-hand parts of the device, respectively, and the strain of the PTFE membrane will result in the change of both C_1 and C_2. In the initial separation state, as illustrated in figure 2(a), the output voltage is decided by the surface charge density and the distance between two electrodes. The open-circuit voltage is given as [26].

$$V_{oc} = \frac{Q}{C_1 + C_2} = \frac{\sigma d}{\varepsilon \varepsilon_0} \quad (1)$$

where d is the distance between two tribo-surfaces, ε_0 is the free space permittivity, ε is the relative permittivity, and σ is the induced surface charge density. We used the output voltage to characterize the response of the TES to an object, which is defined as the difference of the open-circuit voltage

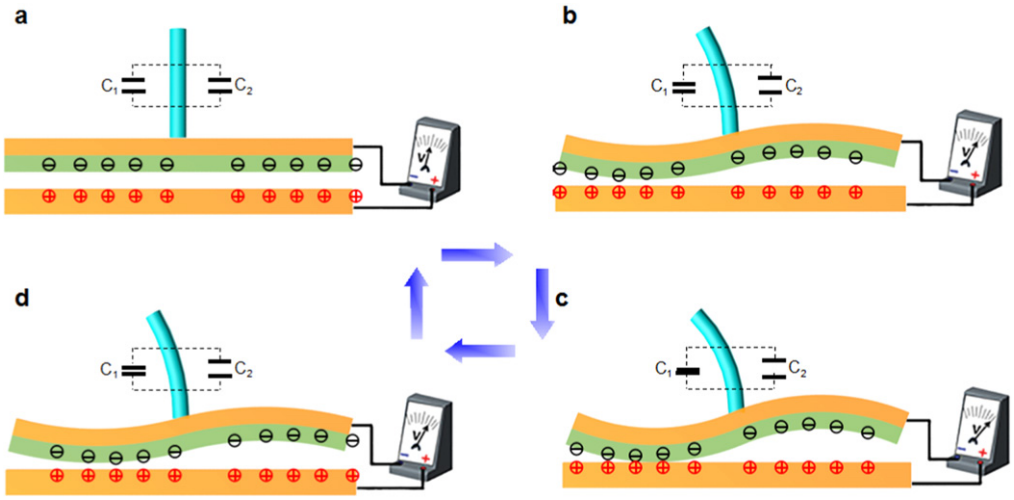

Figure 2. Full cycle of the electricity generation process of the TES.

with respect to that at the separation state. There is a zero-baseline corresponding to the separation state by letting the electrometer be set to zero. Consequently, considering that the Cu contact face and the Cu electrodes are connected to the positive and the negative terminals of a measurement system, the output voltage always has a positive value. When the whisker contacts detect an object and is deflected/bent, the PTFE membrane will buckle. Then, as can be seen in figure 2(b), the left-hand part of the PTFE gradually approaches the Cu electrode, while the right-hand part of the PTFE will swell to the higher position. Accordingly, the C_1 of the left part will be decreased and C_2 of the right part will be increased. The total capacitance between PTFE and the Cu electrode will show a slight change during this process. Corresponding, the output voltage has a slow increase. With an increase of strain, the left part of the PTEF contacts with the Cu electrode and charge neutralization will happen as shown in figure 2(c). Therefore, the left-hand part of the device does not contribute to the output voltage due to the charge neutralization and the output voltage is only decided by the right part of the device. Here, we assume that the surface charge density will not be changed at this contact position due to a good insulating performance of PTFE. The effective capacitance between two tribo-surfaces is only decided by the C_2' of right part. The open-circuit voltage is

$$V_{oc}{}' = \frac{Q}{C'_2} = \frac{\sigma d'_2}{\varepsilon\varepsilon_0} \tag{2}$$

where d_2' are the distance between two tribo-surfaces for the right part of the device (C_2'). Since the distance d_2' is increased in comparison with d_2 in the first stage, the output voltage will also be increased accordingly. If the strain of the whisker continues and the deformation of the PTFT membrane doesn't reached its elastic limit, the increasing of output voltage will go on until the PTFE membranes wells at the highest point. At this time, the output voltage reaches its maximum value. When the whisker leaves the object, the two parts of the PTFE move toward to the initial state. In response to the reduced separation, the output voltage drops (figure 2(d)). Finally, the strain is released and the tribo-electric charge distribution is restored to the original status (figure 2(a)). This is a complete cycle of electricity generation. We have designed and conducted a series of measurements to characterize the performance of the TES, as discussed next.

The performance of the TES sensitively depends on the size of the whisker. Therefore, the open-circuit voltage (V_{oc}) and the short-circuit current (I_{sc}) of the sensor with different aspect ratios (ARs) of 72, 100, and 136 were measured first under the same tip displacement, respectively, as shown in figures 3(a) and (b). It can be seen that with the decrease of AR, the V_{oc} and I_{sc} are all enhanced. Enhancements of V_{oc} and I_{sc} by a factor of 7.2 and 8, respectively, are obtained for the device with an AR value of 72 compared to that of 136. This result indicates TES that under the same tip displacement, the smaller (short and thick) the AR is, the more sensitive the TES is. However, it is to be noted that the V_{oc} and I_{sc} are notably saturated under small AR of 72, as marked in figure 3. Such saturation is caused because the deformation of the PTFT membrane has reached its elastic limit, which makes triboelectric charges on the membrane have little influence on the electric field distribution. Consequently, TES could not sense all the strain induced by the object and missed part of the information about the object. While, if the AR is too large (long and thin), the sensitivity will lower and weaken the sensing capability of TES. As a result, an optimum AR is needed to maximize the sensing capability and benefit the resolution.

Upon the optimization of device design with appropriate AR (length of 11 mm and radius of 120 μm), a further step is made toward investigating the basic performance of the TES for tactile discrimination. The repetition of TES was first measured under periodic deflecting the whisker laterally, as illustrated in figure 4(a). The standard deviation is 8 mV, which indicates that the TES has a good repetition. Figure 4(b) gives the relationship between the V_{oc} and the tip displacement d. Based on the experimental results, a fitting renders a linear relationship between the V_{oc} and d, which can

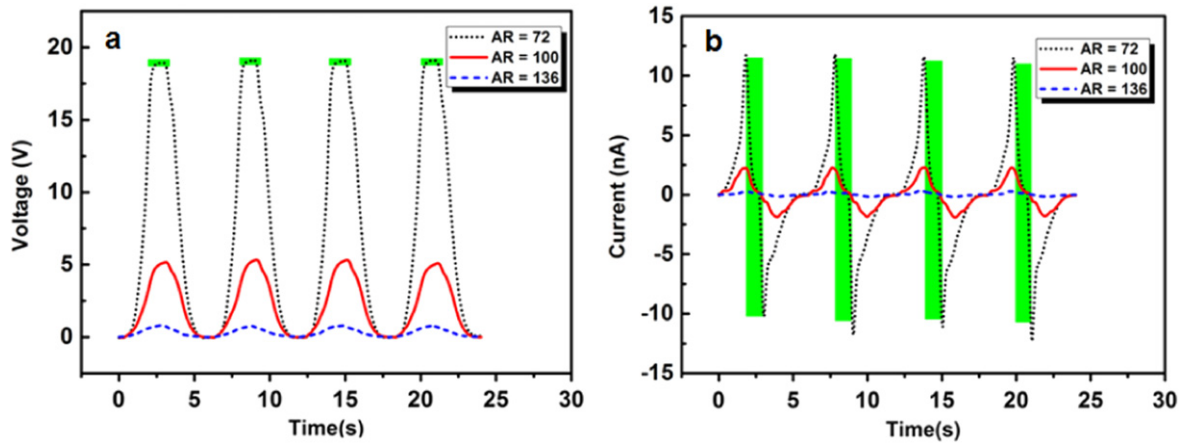

Figure 3. Electrical measurement of the sensor. (a) V_{OC} and (b) I_{SC} under different ARs of whiskers (AR = 72, 100, and 136).

be expressed as

$$V_{oc} = 0.45d - 0.0008 \quad (3)$$

The sensitivity of the TES was as high as 0.45 V mm^{-1} in the displacement range from 0 to 4 mm at a velocity of 1 mm s^{-1}. The high sensitivity of the TES is attributed to the unique electricity generation mechanism introduced previously, which ensures it detects a weak signal without using an electrical amplifier. When the TES is used for tactile recognition, characterizing its resolution is necessary. Figures 4(c) and (d) display the lateral resolution and Z-direction resolution of the TES. A surface profiler was used as a referred sensor. The information of a stair-like object (see input shape) with the same height obtained by the TES and surface profiler was illustrated in figure 4(c). To evaluate the lateral resolution, we used the normalized least mean square adaptive filter to deconvolute the measured data. The calculated value is about 250 μm (see figure S1). Comparing the response of two sensors, we can see that the starting signal and end signal of every stair obtained by the surface profiler are much sharper than that obtained by TES, which is consistent with the lateral resolution of two sensors. Moreover, it can be seen that the TES can easily detect the height of 58 μm and the high output voltage of 1.1 V was obtained, which reveals its Z-direction resolution limit is better than 58 μm. The higher Z-direction resolution 18 μm is given when the TENG scans a printed circuit board. The distorted response of TES is also due to its lower lateral resolution. Even so, the spatial resolution of TES is higher than that of human fingertips of ~1 mm [27] and can be used as a high sensitive tactile sensor. In this study, the spatial resolution of the sensor is determined not only by the Young's modulus of the material, shape, and size of the whisker and mechanical/electrical conversion capability of TENG, but also by the scanning mode and amplifying capability of the measurement equipment.

With superior basic performance, the TES used for surface topography imaging working in a self-powered mode is demonstrated. Figures 5(a) and (b) first exhibit the capability of the TES to reveal the surface feature of the detected object. Figure 5(a) gives the electrical response of the sensor to a flat acrylic plate. As illustrated in the insert, there is an increased electrical output when the flat acrylic plate starts to contact the whisker from the lateral side. Then, a flat and stable electrical signal is observed when the whisker slides on the surface of the acrylic plate because of no distance change between the two electrodes. Finally, a drop of electrical signal is detected due to the release of strain when the whisker slips over the edge of the plane. The obtained electrical signal is consistent with the surface feature of the plate. Representative signals when the sensor sweeps over an acrylic plate with five holes with equal diameter and equal space are shown in figure 5(b). The measurement condition similar to that of a flat plate is displayed in the insert. Five oscillated signals corresponding to five holes with equal space and same shape occur in the flat region in figure 5(b). Compared with the signal in figure 5(a), the divergence in electrical signals has a good match with the difference of the two detected objects, which demonstrates that the sensor has a good capacity for distinct surface features. Therefore, from the electrical signal obtained by the TES, one can deduce the surface feature of the object, whether it is flat or pothole. Next, we used the TES to determine the width (or length) and the relative height of the object. Figure 5(c) shows the signals when the TES scans over four stairs with width of 0.95, 2.75, 4.70, and 6.75 mm in parallel, respectively. It can be seen that the signals not only reflect the flat surface feature of stairs, but also give information of the width. The wider the stair is, the longer the time is. According to the results in figure 5(a) and the working mechanism of the sensor, the width of the stairs is equal to the scanning velocity (v) multiplied by the time(s) at which the whisker passes the stairs. The measured widths are shown in figure 5(d) with an error less than 5% for each stair. The capability to determine the relative height of the object is exhibited in figure 5(e) by scanning over four stairs with height of 65, 140, 208, and 272 μm in series, respectively. The electrical signals are similar to that in figure 5(c). The higher the stair is, the larger the voltage is. A relationship between the output voltage and height as shown in figure S2 is needed before deriving the height of a random object. According to the relationship, the

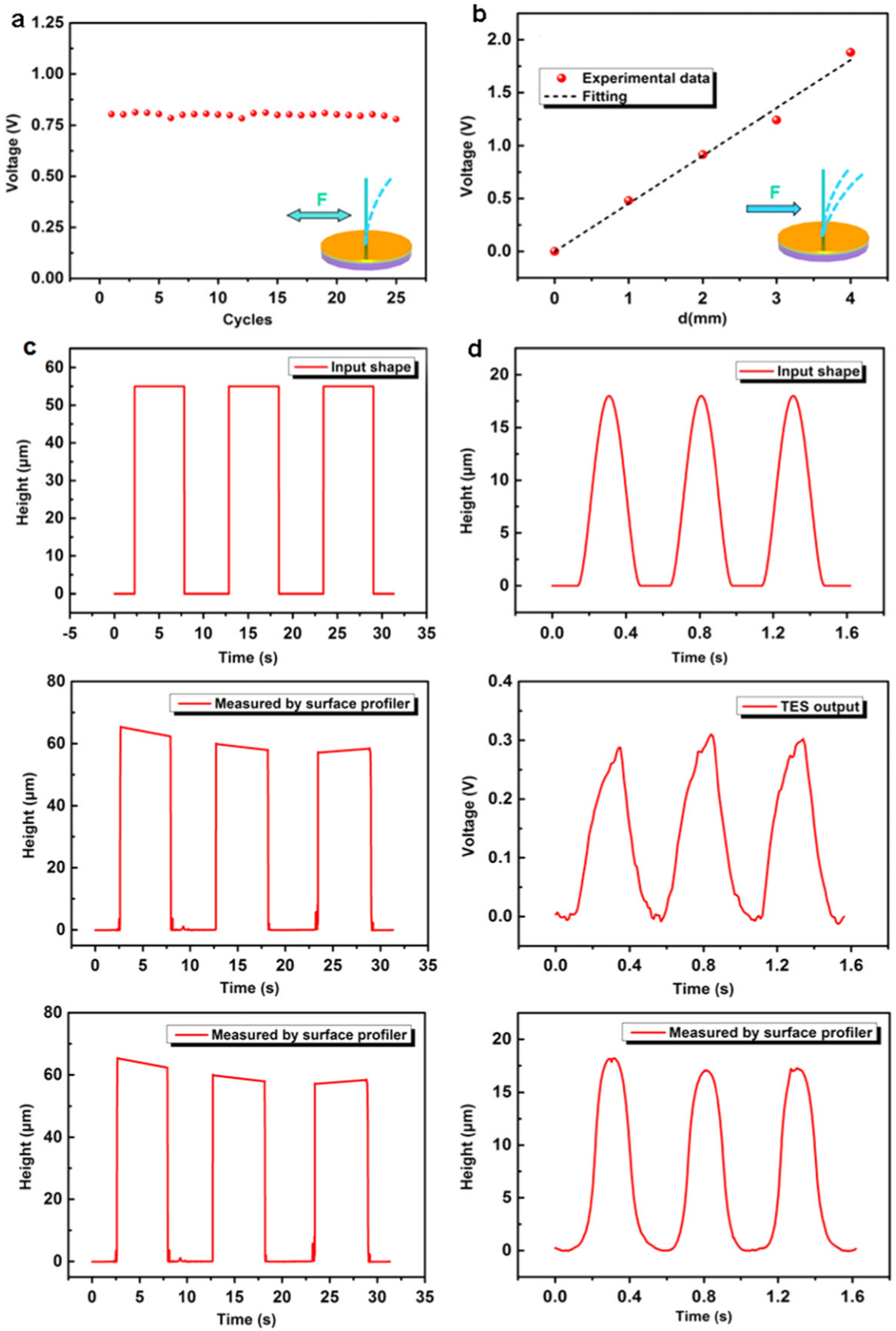

Figure 4. Basic performance of the sensor. (a) Stability of the sensor. The insert is the experimental process. (b) The relationship between the output voltage of the sensor and tip displacement (d). (c) The lateral resolution of the sensor. A stair-like object was scanned over by TENG and surface profiler, respectively. (d) The normal resolution of the sensor. A printed circuit board was scanned over by TENG and surface profiler, respectively.

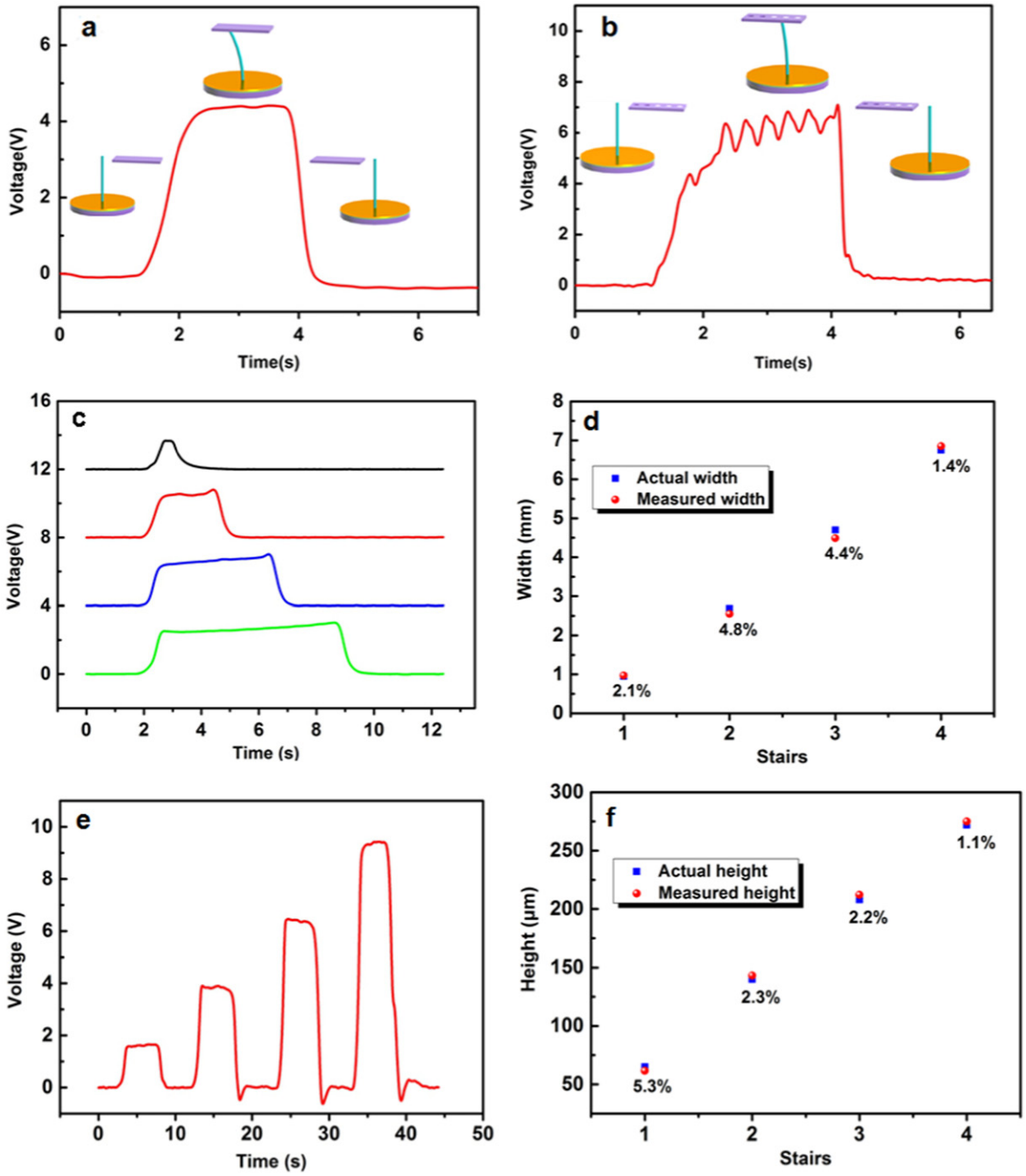

Figure 5. (a) The output voltage signals when the sensor scans over (a) a flat acrylic plate, (b) a flat acrylic plate with five holes with equal diameter and equal space. (c) The output voltage signals when the sensor scans over five flat planes with different widths (0.9, 2.7, 4.7, 6 mm) and (d) object width extraction. (e) The output voltage signals when the sensor scans over stairs with five steps (65, 140, 208, 272 μm) and (f) object height extraction.

deduced height is shown in figure 5(f) with an error less than 5.5% for each stair. As described in figure 4, the error is also greatly related to the sensitivity of TES and the material and size of the whisker. The accuracy is expected to be much better than this with higher Z-direction resolution and lateral resolution.

On the basis of the results in figure 5, we demonstrated the two-dimensional (2D) and three-dimensional (3D) surface topography imaging capability of the TES by multiple scanning. A schematic illustration of the measurement is shown in figure 6(a). Letters 'T', 'E', 'N' and 'G' with same width of 60 mm and same length of 75 mm were scanned separately. A mechanical linear motor was used to realize the reciprocating motion of the scan. Every letter was scanned 26 times to cover the whole surface topography. Figure 6(b) is the background signal with no contact between the whisker and letter. The inset is a color plot of the output voltage for all the measurements in this figure. Figure 6(c) shows a 2D

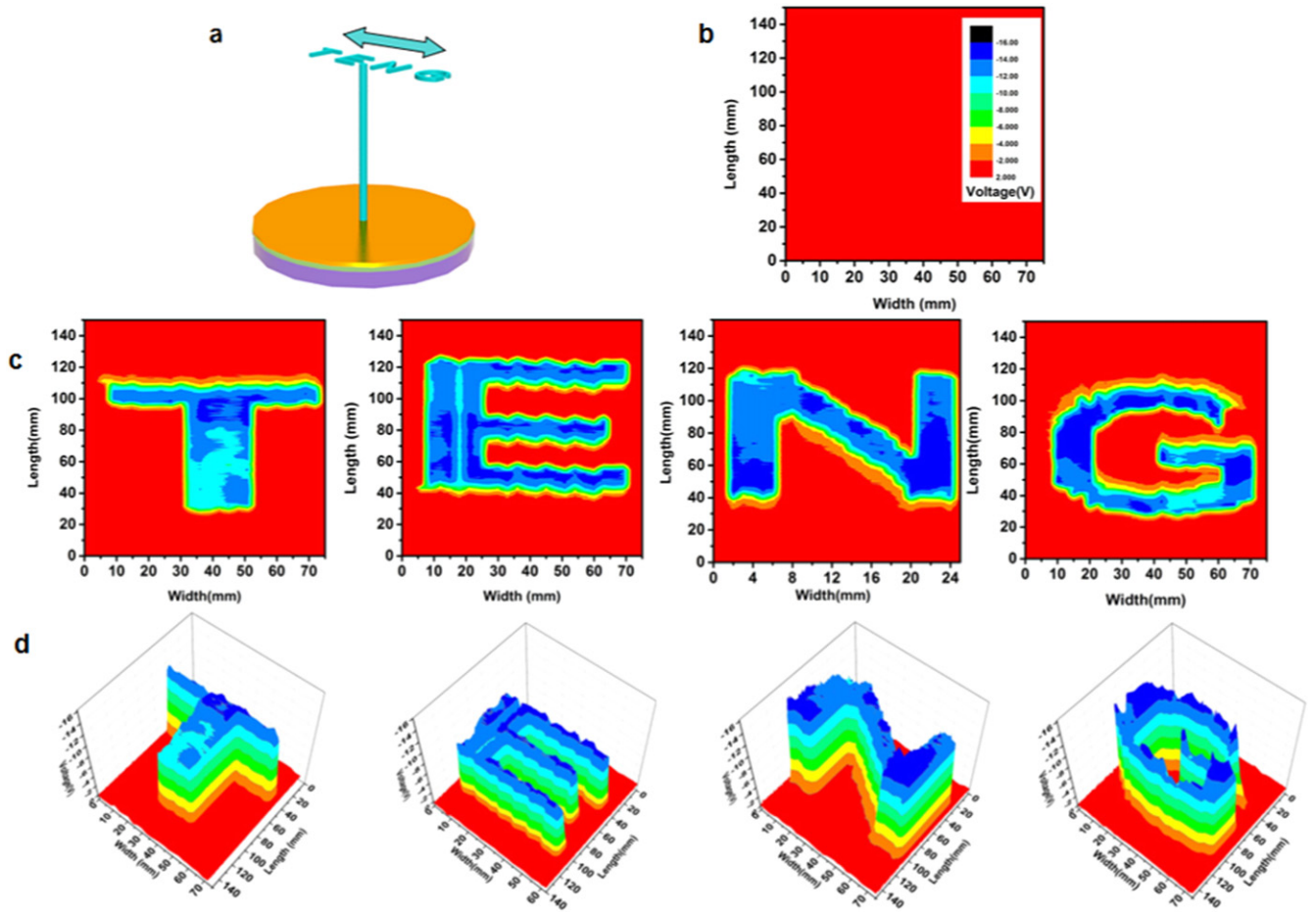

Figure 6. (a) A schematic illustration of the measurement. (b) The background signal with no contact between the whisker and object. The inset is color scaling of voltage for all the measurements in this figure. (c) The 2D and (d) 3D mapping result by scanning over 'T', 'E', 'N', and 'G' shown in (a), respectively.

morphology plotting of the four letters. The width, length, and flat surface feature of letters can also be obtained from the 2D mapping. The information well reflects the true topography of the letters. Furthermore, lively 3D mappings of these letters are illustrated in figure 6(d). The letters have the same height, 1.2 mm, which is given in figure S3. The results in figure 6(d) demonstrated that the TES has the ability to provide a 3D topographic profile of the detected object.

Conclusions

By using a TENG and an artificial whisker, we developed a self-powered signal reading approach without supplying an external power or light source. On the basis of coupling contact-electrification effect and electrostatic induction, the deflection of the whisker causes the two contacting surfaces of the TENG to give an electric output current/voltage that responds to the bending degree of the whisker when it scans over a rough surface. The concept and design of TES could be interesting for developing a self-powered scanning probe for surface topography imaging at relatively low spatial resolution.

Acknowledgments

Our research was supported by the 'Thousands Talents' Program for Pioneer Researcher and his innovation team, China and the Beijing City Committee of Science and Technology: Z131100006013004. We also thank Chao Yuan, Tao Jiang, Weiming Du, Limin Zhang, and Xiaohui Li for their technical assistance.

References

[1] Kim D-H, Lu N, Ma R, Kim Y-S, Kim R-H, Wang S, Wu J, Won S M, Tao H and Islam A 2011 Epidermal electronics *Science* **333** 838–43

[2] Dargahi J and Najarian S 2005 Advances in tactile sensors design/manufacturing and its impact on robotics applications–a review *Ind. Robot* **32** 268–81

[3] Schwartz G, Tee B C, Mei J, Appleton A L, Kim do H, Wang H and Bao Z 2013 Flexible polymer transistors with high pressure sensitivity for application in electronic skin and health monitoring *Nat. Commun.* **4** 1859

[4] Macleod C N, Pierce S G, Sullivan J C, Pipe A G, Dobie G and Summan R 2013 Active whisking-based remotely deployable NDE sensor *IEEE Sens. J.* **13** 4320–8

[5] Bebek O and Cavusoglu M C 2008 Whisker-like position sensor for measuring physiological motion *IEEE-ASME T. Mech.* **13** 538–47
[6] Asadnia M, Kottapalli A G P, Shen Z Y, Miao J M and Triantafyllou M 2013 Flexible and surface-mountable piezoelectric sensor arrays for underwater sensing in marine vehicles *IEEE Sensors J.* **13** 3918–25
[7] Kottapalli A, Asadnia M, Hans H, Miao J and Triantafyllou M 2014 Harbor seal inspired MEMS artificial micro-whisker sensor *27th Int. IEEE Conf. on Micro Electro Mechanical Systems* pp 741–4
[8] Schwartz G, Tee B C K, Mei J G, Appleton A L, Kim D H, Wang H L and Bao Z N 2013 Flexible polymer transistors with high pressure sensitivity for application in electronic skin and health monitoring *Nat. Commun.* **4** 1859
[9] Boland J J 2010 FLEXIBLE ELECTRONICS Within touch of artificial skin *Nat. Mater.* **9** 790–2
[10] Song Y M *et al* 2013 Digital cameras with designs inspired by the arthropod eye *Nature* **497** 95–9
[11] Harada S, Honda W, Arie T, Akita S and Takei K 2014 Fully printed, highly sensitive multifunctional artificial electronic whisker arrays integrated with strain and temperature sensors *ACS Nano* **8** 3921–7
[12] Dehnhardt G, Mauck B and Bleckmann H 1998 Seal whiskers detect water movements *Nature* **394** 235–6
[13] Vincent S B 1912 The functions of the vibrissae in the behavior of the white rat *Behav. Monograph.* **1** 7–81
[14] Dehnhardt G and Ducker G 1996 Tactual discrimination of size and shape by a California sea lion (Zalophus californianus) *Anim. Learn. Behav.* **24** 366–74
[15] Stocking J B, Eberhardt W C, Shakhsheer Y A, Calhoun B H, Paulus J R and Appleby M 2010 A Capacitance-based whisker-like artificial sensor for fluid motion sensing *IEEE Sensor* **143** 2224–9
[16] Heo J S, Chung J H and Lee J J 2006 Tactile sensor arrays using fiber Bragg grating sensors *Sensors Actuators* A **126** 312–27
[17] Dahiya R S, Metta G, Valle M, Adami A and Lorenzelli L 2009 Piezoelectric oxide semiconductor field effect transistor touch sensing devices *Appl. Phys. Lett.* **95** 034105
[18] Fan F R, Tian Z Q and Wang Z L 2012 Flexible triboelectric generator! *Nano Energy* **1** 328–34
[19] Han C B, Zhang C, Li X H, Zhang L, Zhou T, Hu W and Wang Z L 2014 Self-powered velocity and trajectory tracking sensor array made of planar triboelectric nanogenerator pixels *Nano Energy* **9** 325–33
[20] Zhang H L, Yang Y, Hou T C, Su Y J, Hu C G and Wang Z L 2013 Triboelectric nanogenerator built inside clothes for self-powered glucose biosensors *Nano Energy* **2** 1019–24
[21] Fan F R, Lin L, Zhu G, Wu W Z, Zhang R and Wang Z L 2012 Transparent triboelectric nanogenerators and self-powered pressure sensors based on micropatterned plastic *Nano Lett.* **12** 3109–14
[22] Chen M X, Li X Y, Lin L, Du W M, Han X, Zhu J, Pan C F and Wang Z L 2014 Triboelectric nanogenerators as a self-powered motion tracking system *Adv. Funct. Mater.* **24** 5059–66
[23] Yang J, Chen J, Liu Y, Yang W Q, Su Y J and Wang Z L 2014 Triboelectrification-based organic film nanogenerator for acoustic energy harvesting and self-powered active acoustic sensing *ACS Nano* **8** 2649–57
[24] Zhang H, Yang Y, Su Y, Chen J, Adams K, Lee S, Hu C and Wang Z L 2014 Triboelectric nanogenerator for harvesting vibration energy in full space and as self-powered acceleration sensor *Adv. Funct. Mater.* **24** 1401–7
[25] Zhou Y S, Liu Y, Zhu G, Lin Z-H, Pan C, Jing Q and Wang Z L 2013 *In situ* quantitative study of nanoscale triboelectrification and patterning *Nano Lett.* **13** 2771–6
[26] Niu S, Liu Y, Wang S, Lin L, Zhou Y S, Hu Y and Wang Z L 2013 Theory of sliding-mode triboelectric nanogenerators *Adv. Mater.* **25** 6184–93
[27] Van Boven R W and Johnson K O 1994 The limit of tactile spatial resolution in humans grating orientation discrimination at the lip, tongue, and finger *Neurology* **44** 2361